
On Implicit Regularization in β -VAEs

Abhishek Kumar

abhishek@google.com

Google Research

Ben Poole

pooleb@google.com

Google Research

Abstract

While the impact of variational inference (VI) on posterior inference in a fixed generative model is well-characterized, its role in regularizing a learned generative model when used in variational autoencoders (VAEs) is poorly understood. We study the regularizing effects of variational distributions on learning in generative models from two perspectives. First, we analyze the role that the choice of variational family plays in imparting uniqueness to the learned model by restricting the set of optimal generative models. Second, we study the regularization effect of the variational family on the local geometry of the decoding model. This analysis uncovers the regularizer implicit in the β -VAE objective, and leads to an approximation consisting of a deterministic autoencoding objective plus analytic regularizers that depend on the Hessian or Jacobian of the decoding model, unifying VAEs with recent heuristics proposed for training regularized autoencoders. We empirically verify these findings, observing that the proposed deterministic objective indeed exhibits similar behavior to the β -VAE in terms of objective value and sample quality on CelebA and MNIST.

data (Bengio et al., 2013). However, without additional assumptions it may not be possible to recover or identify the correct model (Hyvärinen & Pajunen, 1999; Locatello et al., 2019).

We study the regularization effects of variational posteriors on the learned generative model from two perspectives. First, we discuss the role of *the choice of variational family* in imparting uniqueness properties to the learned generative model by restricting the set of possible solutions. We argue that restricting the variational family in specific ways can rule out non-uniqueness to a corresponding set of transformations on the generative model. Next, we study the regularization effect of variational family on the geometry of the decoding model ($p_\theta(x|z)$) in β -VAE. We characterize this effect in the case where the variational family is the location-scale family (e.g., Gaussian). This enables us to understand the effect of posterior covariance structure on the Jacobian matrix of the decoding model. In the particular case of Gaussian prior and posterior, we further use this relation to derive a deterministic objective that closely approximates the β -VAE objective.

We perform experiments to validate the correctness of our theory and accuracy of our approximations. On the MNIST dataset, we empirically verify the relationship between posterior covariance and the Jacobian of the decoder. In particular, we observe that block-diagonal posterior covariance encourages a block diagonal structure on the matrices $J_g(z)^\top J_g(z)$ where $J_g(z)$ is the decoder Jacobian matrix. This can be seen as generalizing the results from recent work (Rolinek et al., 2019) which showed (via different proof techniques) that for Gaussian observation models, *diagonal* Gaussian approximate posteriors result in orthogonal Jacobians. We also compare the objective values of the original β -VAE objective with our derived deterministic objectives. While our deterministic approximation holds for small β , we find that the two objectives remain in agreement for a reasonably wide range of β . We also train models using a tractable lower bound on the deterministic objectives and

1. Introduction

Variational autoencoders (VAEs) (Kingma & Welling, 2013; Rezende et al., 2014) and its variants such as β -VAE (Higgins et al., 2017; Alemi et al., 2017) are popular models for density estimation and posterior inference, and for learning representations and generative samplers of data. Learning such latent-variable models provides an attractive mechanism for capturing the underlying data-generating process that created a dataset: ideally the latent variables can have a simple correspondence to the factors of variation in the

find that trained models behave similar to β -VAE in terms of sample quality when varying β .

2. Latent-variable models and identifiability

We begin by discussing identifiability in latent-variable models, and the role that the choice of variational family plays in regularizing and restricting the set of optimal models.

Latent-variable models. We consider latent-variable generative models that consist of a fixed prior $p(z)$, and a conditional generative model or *decoder*, $p_\theta(x|z)$. In maximum-likelihood estimation, we aim to maximize the marginal log-likelihood of the training data, $\log p_\theta(x) = \log \int dz p_\theta(z) p_\theta(x|z)$ in terms of the parameters θ . We will sometimes omit explicit dependence on parameters θ for brevity. A desirable goal in learning latent-variable models is that the learned latent variables, z , correspond simply to “ground-truth factors of variation” that generated the dataset (Bengio et al., 2013; Higgins et al., 2017). For example, in a dataset of shapes we aim to learn latent variables that are in one-to-one correspondence with attributes of the shape like size, color, and position. Learning such “disentangled” representations may prove useful for downstream tasks such as interpretability and few-shot learning (Gilpin et al., 2018; van Steenkiste et al., 2019).

Identifiability and non-uniqueness. Unfortunately, there is an inherent identifiability issue with latent-variable models trained with MLE: there are typically a large set of models that have the same marginal data and prior distributions, $p_\theta(x)$ and $p_\theta(z)$, but entirely different latent variables z . Thus identifying the “right” model whose latents are in one-to-one correspondence with factors of variation is not feasible with MLE alone. In our work, we adopt the definition of identifiability from the ICA literature that ignores permutations and nonlinear transformations that act separately on each latent dimension (Hyvärinen & Pajunen, 1999). This identifiability issue is well-known in the ICA literature (Hyvärinen & Pajunen, 1999) and causal inference literature (Peters et al., 2017), and has been highlighted more recently in the context of learning disentangled representations with factored priors (Locatello et al., 2019).

More formally, we can find transformations r of the latent variable z that leave its marginal distribution $p(z)$ the same, and thus the marginal data distribution $p(x)$ the same. The transformation r is not just a simple permutation or nonlinear transformation of individual latents, but *mixes* components of the latent representation, breaking the requirement for identifiability as defined previously. This leads to a *set* of solutions instead of a *unique* solution, all of which are equal according to their marginal log-likelihood, but that have distinct representations.

Non-uniqueness for factorized priors. For models with

continuous factorized priors, $p(z) = \prod_i p_i(z_i)$, Locatello et al. (2019) present a construction of transformations r that mix latents but leave the marginal data distribution unchanged. We summarize it here for completeness and also extend it to the case of non-factored priors which was conjectured but not covered in (Locatello et al., 2019). The construction first transforms all marginal distributions $p_i(z_i)$ to uniform distributions by the mapping $u_i = F_i(z_i)$ where $F_i(\cdot)$ is the c.d.f. corresponding to the density $p_i(\cdot)$. This independent uniform random vector u is then transformed to independent standard normal random vector by the mapping $n_i = \psi^{-1}(z_i)$ where $\psi(\cdot)$ is the c.d.f. of the standard normal. As the r.v. n is independent standard normal distributed and thus spherically symmetric, for any orthogonal transformation U , the transformed r.v. $z' = r(z) = (F^{-1} \circ \psi \circ U \circ \psi^{-1} \circ F)(z)$ has same density as the prior $p(z)$ while completely mixing the latent variables z (*i.e.*, the transform has Jacobian $J_r(z)$ with nonzero off-diagonals, with $|\det J_r(z)| = 1$). The marginal observation density $p(x)$ remains unchanged as well, since $p'(x) = \int p(z) p(x|r(z)) dz = \int p(r^{-1}(z')) p(x|z') dz' = \int p(z') p(x|z') dz' = p(x)$.

Non-uniqueness for correlated priors. Although not discussed in Locatello et al. (2019), it is also possible to generalize this construction to *non-factorized* priors by replacing transformations $u_i = F_i(z_i)$ in the first step with $u_i = F_{i|1...(i-1)}(z_i, z_1, \dots, z_{i-1})$ (and its inverse in the last step), where $F_{i|1...(i-1)}$ is the c.d.f. of the conditional distribution of z_i given *earlier* latents (with arbitrary ordering on the latents) (Darmois, 1951; Hyvärinen & Pajunen, 1999).

These non-uniqueness results are troubling if we care about recovering a model which corresponds to recovering the factors of variation from the data-generating process. As long as there exist many solutions that are all equivalent under marginal likelihood, we will be unable to identify the correct model with marginal likelihood alone.

3. Uniqueness via variational family

In the previous section, we highlighted how there can be an infinite family of latent-variable models that all achieve the same marginal likelihood. Here, we show how additional constraints present in the learning algorithm can restrict the space of solutions leading to uniqueness.

We focus on the impact of posterior regularization (Zhu et al., 2012; Shu et al., 2018) via the choice of variational family on the set of solutions to the β -VAE objective. In variational inference, we optimize not only the generative model, $p(x, z) = p(x|z)p(z)$, but also an approximate posterior, $q(z|x)$. When optimizing over $q(z|x)$, we constrain the distributions to come from some family \mathcal{Q} .

We first consider the case when the true posterior lies in the

variational family \mathcal{Q} . Although there are many latent variable generative models with same marginal data distribution $p(x)$, this equivalence class of models shrinks when we constrain ourselves to models with posteriors $p(z|x) \in \mathcal{Q}$. Consider applying a mixing transform r that preserves the prior distribution of z before feeding it to the decoder: $z' = r(z)$. The transformed posterior is given by:

$$\begin{aligned} p'(z|x) &= \frac{p(x|r(z))p(z)}{p(x)} = \frac{p(x|z')p(r^{-1}(z'))}{p(x)} \\ &= \frac{p(x|z')p(z')}{p(x)} = p(z'|x) = p(r(z)|x), \end{aligned} \quad (1)$$

where we used the facts that $p(z) = p(r(z)) = p(r^{-1}(z))$ and $|\det J_r(z)| = 1$. This implies $p(z|x) = p'(r^{-1}(z)|x)$, *i.e.*, the posterior r.v. is transformed by r^{-1} yielding $p'_{z|x} = r^{-1}\#p_{z|x}$ ¹. If $p_{z|x} \in \mathcal{Q}$ but $p'_{z|x} \notin \mathcal{Q}$, then the best ELBO we can achieve in the transformed model p' is strictly less than the untransformed model p . Thus even though r leaves the marginal data likelihood unchanged, it yields a worse ELBO and thus can no longer be considered an equivalent model under the training objective. The question remains that for a distribution family \mathcal{Q} and a $q \in \mathcal{Q}$, what class of transformations R guarantee that $r^{-1}\#q \notin \mathcal{Q}$ for all $r \in R$? This has to be answered on a case-by-case basis, but we consider an example below.

3.1. Example: Isotropic Gaussian prior and orthogonal transforms

An isotropic Gaussian prior is invariant under orthonormal transformations (characterized by orthogonal matrices with unit norm columns). For a mean-field family of distributions \mathcal{Q} , the necessary and sufficient conditions for $r^{-1}\#p_{z|x} \in \mathcal{Q}$, given $p_{z|x} \in \mathcal{Q}$, for r belonging to the set of orthonormal transformations, are (Skitovitch, 1953; Darrow, 1953; Lukacs et al., 1954): (i) $p_{z|x}$ is a factorized Gaussian, and (ii) variances of the individual latent dimensions of the posterior are all equal. If either of these two conditions are not satisfied, the orthogonal symmetry in the generative model, which arises from using the isotropic Gaussian prior, is broken, and the only orthogonal transforms r allowed on the generative model will be the permutations. This Darrow-Skitovitch characterization of the Gaussian random vectors has also been used to prove identifiability results for linear ICA (Hyvärinen & Pajunen, 1999). However, here we do not need any linearity assumption on the conditional generative model $p(x|z)$.

Probabilistic PCA (Tipping & Bishop, 1999) is one example in this model class with $p(z) = \mathcal{N}(0, I)$, $p(x|z) = \mathcal{N}(Az, \sigma^2 I)$ and $p(x) = \mathcal{N}(0, AA^\top + \sigma^2 I)$, that has Gaus-

¹For clarity, we denote the transformed distribution using push-forward notation: where $f\#p$ denotes the distribution created by transforming samples from p using the deterministic function f .

sian posterior which is factored when A has orthogonal columns. However, there are equivalent models $p(x|z) = (AVz, \sigma^2 I)$ with V orthonormal that yield the same $p(x)$ and still factorized posterior if columns of A have equal norms. This symmetry vanishes only when all columns of A have different norms (condition (ii) mentioned earlier).

3.2. Uniqueness in β -VAE

The choice of variational family can lead to uniqueness even when the true posterior is not in the variational family. Consider optimizing models with the β -VAE objective (Higgins et al., 2017):

$$L(q, p) := \mathbb{E}_{q(z|x)} \log p_{x|z}(x|z) - \beta \text{KL}(q(z|x)||p_z(z)). \quad (2)$$

Note that we maximize the objective w.r.t. only the decoder $p_{x|z}$ (not the prior p_z) but use the shorthand $L(q, p)$ in place of $L(q, p_{x|z})$ for brevity. Let \mathcal{P} denote the set of all generative models with fixed prior p_z but arbitrary decoder $p_{x|z}$. Let R be the class of (deterministic) mixing transforms that leave the prior invariant, *i.e.*, $p_z = r\#p_z$. Note that $r \in R \Rightarrow r^{-1} \in R$. Given a solution (q^*, p^*) , *s.t.*, $(q^*, p^*) = \max_{q \in \mathcal{Q}, p \in \mathcal{P}} L(q, p)$, we would like to know if there is a transformational non-uniqueness associated with it, *i.e.*, if it is possible to transform the generative model by r and get the same marginal $p(x)$ as well as same objective value of (2). The following result gives a condition under which this non-uniqueness is ruled out.

Theorem 1. *Let R be the class of mixing transforms that leave the prior invariant, and p_r be the generative model obtained by transforming the latents of the model p by $r \in R$. Let $L(q^*, p^*) = \max_{q \in \mathcal{Q}, p \in \mathcal{P}} L(q, p)$. Let $\tilde{\mathcal{Q}}$ be the completion of \mathcal{Q} by R , *i.e.*, $\tilde{\mathcal{Q}} = \{r\#q : q \in \mathcal{Q}, r \in R\} \cup \mathcal{Q}$. If \mathcal{Q} is *s.t.* $q \in \mathcal{Q} \Rightarrow r\#q \notin \mathcal{Q}$ for all $r \in R$, and $\arg \max_{q \in \tilde{\mathcal{Q}}} L(q, p^*)$ is unique, then $\max_{q \in \mathcal{Q}} L(q, p_r^*) < L(q^*, p^*)$.*

Proof. Please refer to the Appendix. \square

Corollary 1. *If the set $\tilde{\mathcal{Q}}$ defined in Theorem 1 is convex, then $\arg \max_{q \in \tilde{\mathcal{Q}}} L(q, p^*)$ is unique. When all other assumptions of Theorem 1 are met, we have $\max_{q \in \mathcal{Q}} L(q, p_r^*) < L(q^*, p^*)$.*

Proof. Please refer to the Appendix. \square

Hence, for a choice of variational family \mathcal{Q} such that the tuple (\mathcal{Q}, R) satisfies the condition of Theorem 1, transforming the latents by $r \in R$ will result in decreasing the optimal value of the β -VAE objective, thus breaking the non-uniqueness. From Section 3.1, we know that using a Gaussian prior, and restricting \mathcal{Q} to factorized *non-Gaussian* distributions is one such choice that ensures a

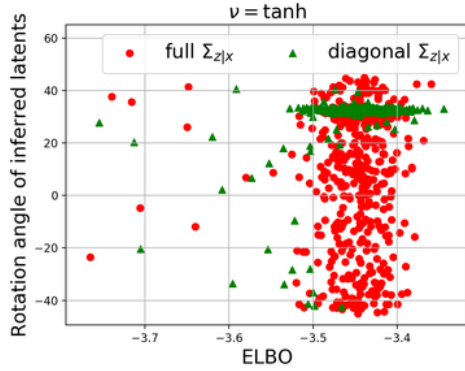


Figure 1. Rotation angle between true latents and inferred latents for VAEs (multiple runs): diagonal Σ encourages unique solution in terms of inferred latents as the ELBO increases. Please refer to text for details. More experiments are provided in the Appendix.

unique (q^*, p^*) when R is the class of orthogonal transformations. Thus the choice of prior and variational family can help to guarantee uniqueness of models trained with the β -VAE objective. We conduct an experiment highlighting this empirically. We generate $4k$ samples in two dimensions using $x = \nu(Wz) + \epsilon$, with $z \sim \mathcal{N}(0, I)$, $\epsilon \sim \mathcal{N}(0, .05^2)$. Entries of $W \in \mathbb{R}^{2 \times 2}$ are sampled from $\mathcal{N}(0, 1)$ and normalized such that columns have different ℓ_2 norms (2 and 1, respectively). ν is either Identity (Probabilistic PCA) or a nonlinearity (tanh, sigmoid, elu). A VAE is trained on this data, with decoder of the form $x = \nu(Az) + b$ and variational posterior of the form $q(z|x) = \mathcal{N}(Cx + d, \Sigma)$ with A, b, C, d and Σ learned. We do multiple random runs of this experiment and measure the rotation angle between true latents and inferred posterior means (after ignoring permutation and reflection of axes so the angle ranges in $(-45, 45]$). Each runs is trained with a varying number of iterations so they reach solutions with varying degrees of suboptimality (ELBO). Fig. 1 shows a scatter plot of rotation angle vs ELBO for $\nu=\text{tanh}$. When Σ is diagonal (mean-field $q(z|x)$), there is a unique solution in terms of inferred latents as the ELBO increases (ignoring the permutations and reflections of latent axes). In the Appendix we show this uniqueness is not due to additional inductive biases in the optimization algorithm, and include results for unamortized VI and other activations ν .

Disentanglement. Locatello et al. (2019); Mathieu et al. (2019) highlight that learning disentangled representations using only unlabeled data is impossible without additional inductive biases due to this non-uniqueness issue of multiple generative models resulting in same $p(x)$. Based on the discussion in this section, it can be seen that the choice of variational family can be one such inductive bias, *i.e.*, it can be chosen in tandem with the prior to rule out issues of non-uniqueness due to certain transforms. Most exist-

ing works on unsupervised disentanglement using β -VAE’s (Higgins et al., 2017; Kumar et al., 2018; Chen et al., 2018; Kim & Mnih, 2018; Burgess et al., 2018) use a standard normal prior and factored Gaussian variational family which should not have this orthogonal non-uniqueness issue (*i.e.*, the construction in Locatello et al. (2019)), unless the variational posterior covariances are all equal. Note that this observation is limited to the theoretical uniqueness aspect of the models and does not contradict the empirical results and conclusions in (Locatello et al., 2019) in any way. Burgess et al. (2018) also discuss how disentangled representations may emerge when using a mean field variational family, but do not present a rigorous argument connected to uniqueness.

4. Deterministic approximations of β -VAE

Next, we analyze how the covariance structure of the variational family can influence the geometry of the learned generative model. We start with the β -VAE objective of Eq. (2), which reduces to the ELBO for $\beta = 1$. We use $p_\theta(x|z)$ to denote the decoding model parameterized by θ , and $q_\phi(z|x)$ to denote the amortized inference model (encoding model) parameterized by ϕ . We will sometimes omit the parameter subscripts for brevity. We explicitly consider the case where the posterior $q_\phi(z|x)$ belongs to the location-scale family of distributions that are reasonably concentrated around the location parameters (*e.g.*, Gaussian distribution with small variance). We denote the latent dimensionality by d and the observation dimensionality by D .

Let us denote $f_x(z) = \log p(x|z)$ and view $\log p(x|z)$ as a scalar function of z for a given x . The second-order Taylor series expansion of $f_x(z)$ around the location parameter $\mu_{z|x} = \mathbb{E}_{q_\phi(\cdot|x)}[z] = h_\phi(x)$ is given by:

$$f_x(z) \approx \log p(x|h_\phi(x)) + J_{f_x}(h_\phi(x))(z - h_\phi(x)) + \frac{1}{2}(z - h_\phi(x))^\top H_{f_x}(h_\phi(x))(z - h_\phi(x)), \quad (3)$$

where $J_{f_x}(z) \in \mathbb{R}^{1 \times d}$ and $H_{f_x}(z) \in \mathbb{R}^{d \times d}$ are the Jacobian and Hessian of f_x evaluated at z . Note that the expectation of the second term under $q_\phi(z|x)$ is zero as $\mathbb{E}_{q_\phi(\cdot|x)}[z] = h_\phi(x)$. Substituting the approximation (3) in the original β -VAE objective (2), we obtain the following approximation

$$L(p, q) \approx \log p_\theta(x|h_\phi(x)) + \frac{1}{2}\text{tr}(H_{f_x}(h_\phi(x))\Sigma_{z|x}) - \beta \text{KL}(q_\phi(z|x)||p(z)), \quad (4)$$

where $\Sigma_{z|x} = \mathbb{E}_{q_\phi(z|x)}[(z - \mu_{z|x})(z - \mu_{z|x})^\top]$ is the posterior covariance. While this objective no longer requires sampling, it involves a Hessian of the decoder, which can be computationally expensive to evaluate. Next we show

how this Hessian can be computed tractably given certain network architectures.

Let $g_\theta : Z \rightarrow \mathbb{R}^D$ denote the deterministic component of the decoder that maps from a latent vector z to the parameters of the observation model (*e.g.*, to means of the Gaussian pixel observations, to probabilities of the Bernoulli distribution for binary images, etc.). We can further expand the Hessian $H_{f_x}(z)$ to decompose it as the sum of two terms, one involving the Jacobian of the decoder mapping $J_g(z) \in \mathbb{R}^{D \times d}$, and the other involving the Hessian of the decoder mapping, as follows:

$$\begin{aligned} H_{f_x}(z) &= \nabla_z^2 \log p(x|z) = \nabla_z^2 \log p(x; g(z)) \\ &= \nabla_z [(\nabla_{g(z)} \log p(x; g(z))) J_g(z)] \\ &= J_g(z)^\top (\nabla_{g(z)}^2 \log p(x; g(z))) J_g(z) + \\ &\quad (\nabla_{g(z)} \log p(x; g(z))) \nabla_z^2 g(z) \end{aligned} \quad (5)$$

It can be noted that $\nabla_z^2 g(z)$ in the second term is almost always zero when the decoder network uses only piecewise-linear activations (*e.g.*, relu, leaky-relu), which is the case in many implementations. Denoting $H_{p_x}(g(z)) = \nabla_{g(z)}^2 \log p(x; g(z))$, this leaves us with

$$H_{f_x}(z) = J_g(z)^\top H_{p_x}(g(z)) J_g(z) \quad (6)$$

In the case of other nonlinearities, we can make the approximation that $\nabla_z^2 g(z)$ is small and can be neglected. Substituting the Hessian $H_{f_x}(z)$ from Eq. (6) into the approximate ELBO (4), we obtain

$$\begin{aligned} \max_{g, h} \log p(x|h(x)) - \beta \text{KL}(q_\phi(z|x)||p(z)) + \\ \frac{1}{2} \text{tr}(J_g(h(x))^\top H_{p_x}(g(h(x))) J_g(h(x)) \Sigma_{z|x}) \end{aligned} \quad (7)$$

The above deductions in (4) and (7), obtained using the second order approximation of $\log p(x|z)$, imply that stochasticity of the posterior translates to regularizers that encourage the *alignment* of $H_{f_x}(h(x))$ and $J_g(h(x))^\top H_{p_x}(g(h(x))) J_g(h(x))$ with posterior covariance $\Sigma_{z|x}$ by maximizing their inner product with it. Note that for observation models that independently model stochasticity at individual pixels (*e.g.*, pixel-wise independent Gaussian, Bernoulli, etc.), the matrix $H_{p_x}(g(h(x)))$ is diagonal and thus efficient to compute. In particular, for independent standard Gaussian observations (*i.e.*, $p(x; g(z)) = \mathcal{N}(g(z), I)$), $H_{p_x}(g(h(x))) = -I$, the identity matrix of size D .

5. Impact of covariance structure of q

The deterministic approximation to the β -VAE objective allows us to study the relationship between the decoder Jacobian and posterior covariance. Lets consider the specific

case of a standard Gaussian prior, $p(z) = \mathcal{N}(0, I)$, and Gaussian variational family, $q_\phi(z|x) = \mathcal{N}(h_\phi(x), \Sigma_{z|x})$. The objective in (4) reduces to

$$\begin{aligned} \log p_\theta(x|h_\phi(x)) + \frac{1}{2} \text{tr}(H_{f_x}(h_\phi(x)) \Sigma_{z|x}) - \\ \frac{\beta}{2} (\|h_\phi(x)\|^2 + \text{tr}(\Sigma_{z|x}) - \log |\Sigma_{z|x}| - d), \end{aligned} \quad (8)$$

where $|\Sigma_{z|x}|$ denotes the absolute value of the determinant of $\Sigma_{z|x}$. We consider the case when the mean of the posterior is parameterized by a neural network but the covariance is not amortized. The objective (8) is concave in $\Sigma_{z|x}$, and maximizing it w.r.t. $\Sigma_{z|x}$ gives

$$\begin{aligned} \frac{1}{2} H_{f_x}(h_\phi(x)) - \frac{\beta}{2} (I - \Sigma_{z|x}^{-1}) = 0 \\ \implies \Sigma_{z|x} = \left(I - \frac{1}{\beta} H_{f_x}(h_\phi(x)) \right)^{-1} \end{aligned} \quad (9)$$

Substituting Eq. (9) into (8), we get the maximization objective of

$$\begin{aligned} \max \log p_\theta(x|h_\phi(x)) - \frac{\beta}{2} \|h_\phi(x)\|^2 - \\ \frac{\beta}{2} \log \left| I - \frac{1}{\beta} H_{f_x}(h_\phi(x)) \right|. \end{aligned} \quad (10)$$

Following similar steps for the objective (7) gives the optimal posterior covariance of

$$\Sigma_{z|x} = \left(I - \frac{1}{\beta} J_g(h(x))^\top H_{p_x}(g(h(x))) J_g(h(x)) \right)^{-1}, \quad (11)$$

and the maximization objective of

$$\begin{aligned} \max \log p_\theta(x|h_\phi(x)) - \frac{\beta}{2} \|h_\phi(x)\|^2 - \\ \frac{\beta}{2} \log \left| I - \frac{1}{\beta} J_g(h_\phi(x))^\top H_{p_x}(g_\theta(h_\phi(x))) J_g(h_\phi(x)) \right|. \end{aligned} \quad (12)$$

This analysis yields an **interesting** interpretation of the β -VAE objective as a deterministic reconstruction term ($p_\theta(x|h_\phi(x))$), a regularizer on the encodings ($\|h_\phi(x)\|^2$), and a regularizer involving the Jacobian of the decoder mapping.

5.1. Regularization effect of the covariance

The relation between the optimal $\Sigma_{z|x}$ and the Jacobian of the decoder $J_g(z)$ in Eq. (11) uncovers how the choice of the structure of $\Sigma_{z|x}$ influences the Jacobian of the decoder. For example, having a diagonal structure on the covariance matrix (mean-field posterior) should drive

the matrix $(J_g(h(x))^\top H_{p_x}(g(h(x)))J_g(h(x)))$ towards a diagonal matrix. As mentioned earlier, for observation models that independently model the individual pixels given the decoding distribution parameters $g(z)$, the matrix $H_{p_x}(g(z))$ is diagonal which implies that the matrix $|H_{p_x}(g(h(x)))|_{\text{abs}}^{1/2} J_g(h(x))$ is encouraged to have orthogonal columns, where $|H_{p_x}(g(h(x)))|_{\text{abs}}$ denotes taking elementwise absolute values of the matrix $H_{p_x}(g(h(x)))$.

For standard Gaussian observations, we have $H_{p_x}(g(z)) = -I$ for all z , implying that the decoder Jacobian $J_g(h(x))$ will be driven towards having orthogonal columns. For Bernoulli distributed pixel observations, the i 'th diagonal element of matrix $H_{p_x}(g(h(x)))$ is given by $-1/(1 - x_i - [g(h(x))]_i)^2$, where $x_i \in \{0, 1\}$ is the i 'th pixel and $[g(h(x))]_i$ is the predicted probability of i 'th pixel being 1. When the decoding network has the capacity to fit the training data well, *i.e.*, $(1 - x_i - [g(h(x))]_i)^2$ is close to 1 for all i , the Jacobian matrix $J_g(h(x))$ will still be driven towards having orthogonal columns. As is evident from Eq. (11), more interesting structures on the decoder Jacobian matrix can be encouraged by placing appropriate sparsity patterns on $\Sigma_{z|x}^{-1}$. Often it may be expensive to encode constraints on the decoder Jacobian directly, as that would typically require computing the Jacobian to apply the constraint. Instead, this relationship highlights that we can impose soft constraints on the decoder Jacobian by restricting the covariance structure for the variational family.

5.2. Connection with Riemannian metric

For Gaussian observations, Eq. (11) reduces to $\Sigma_{z|x} = \left(I + \frac{1}{\beta} J_g(h(x))^\top J_g(h(x))\right)^{-1}$. The decoder, $g : Z \rightarrow \mathbb{R}^D$, outputs the mean of the distribution and its image $M = g(Z) \subset \mathbb{R}^D$ is an embedded differentiable manifold² of dimension d , when $J_g(z)$ is full rank for all z . If we inherit the Euclidean geometric structure from \mathbb{R}^D , restricting the inner product to the tangent spaces $T_x M$ gives us a Riemannian metric on M . The pullback of this metric to Z gives the corresponding Riemannian metric on Z , which is given by a symmetric positive-definite matrix field $G(z) = J_g(z)^\top J_g(z)$. Recent work has used this metric to study the geometry of deep generative models (Shao et al., 2018; Chen et al., 2017; Arvanitidis et al., 2017; Kuhnel et al., 2018). Given the relation in Eq. (11), we can think of posterior covariance as indirectly inducing a metric on the latent space for Gaussian observations as $G(z) = J_g(z)^\top J_g(z) = \beta(\Sigma_{z|x}^{-1} - I)$ for $z = h(x)$. It will

²This assumes that the decoder uses differentiable nonlinearities which does not hold for piecewise-linear activations such as relu, leaky-relu. However, in principle, they can always be approximated arbitrarily closely by a smooth function for the sake of this argument.

be interesting to investigate the metric properties of $\Sigma_{z|x}^{-1}$ in the context of deep generative models, *e.g.*, for geodesic traversals, curvature calculations, etc. (Shao et al., 2018; Chen et al., 2017).

5.3. Training deterministic approximations of β -VAE

Beyond the theoretical understanding of the implicit regularization in β -VAE, it should also be possible to use the proposed objectives for training the models, particularly when the observation dimensions are conditionally independent as the Hessian $H_{p_x}(\cdot)$ is diagonal. This will also help in investigating the accuracy and utility of our deterministic approximations to the β -VAE objective. We consider the case of Gaussian observation model for simplicity as the matrix $H_{p_x}(g(z)) = -I$, reducing the objective to:

$$\min_{g,h} \frac{1}{2} \|x - g(h(x))\|^2 + \frac{\beta}{2} \|h(x)\|^2 + \frac{\beta}{2} \log \left| I + \frac{1}{\beta} J_g(h(x))^\top J_g(h(x)) \right|. \quad (13)$$

We refer to the objective (13) as Gaussian Regularized AutoEncoder (**GRAE**). However, for large latent dimensions, computing full Jacobian matrices can substantially increase the training cost. To reduce this cost, we propose training with a stochastic approximation of an upper bound of the regularizers in objectives (12) and (13). We use Hadamard inequality for determinants of positive definite matrices A , *i.e.*, $\det(A) \leq \prod_i A_{ii}$ with equality for diagonal A , and approximate the regularizer of (13) as:

$$\log \left| I + \frac{1}{\beta} J_g(h(x))^\top J_g(h(x)) \right| \leq \sum_i \log \left(1 + \frac{1}{\beta} \|[J_g(h(x))]_{:i}\|_2^2 \right) \quad (14)$$

Let p_c be a discrete distribution on the column indices of the Jacobian matrix (*e.g.*, uniform distribution). We can approximate the summation by sampling k column indices $\{c_i\}_1^k$ from the distribution p_c and using $\frac{1}{k} \sum_{i=1}^k \frac{1}{p_c(c_i)} \log \left(1 + \frac{1}{\beta} \|[J_g(h(x))]_{:c_i}\|_2^2 \right)$. In lack of any more information, we simply use a uniform distribution for p_c , and $k = 1$ in all our experiments. We refer to the objective with this more tractable regularizer as **GRAE**_≈. Similar steps can be followed for the regularizer in (12). The upper bound in (14) should be tight for mean-field variational posteriors by virtue of the relation in Eq. (11). For such cases (*i.e.*, sparse posterior precision matrices, including, diagonal), we can impose an additional orthogonal penalty on the corresponding Jacobian columns (in line with Eq. (11)) by penalizing their normalized dot products. This can also be implemented in stochastic form by sampling a pair of Jacobian columns.

It is possible to relate the regularizer in (13) with earlier work on regularized autoencoders. We can use the Taylor series for $\log(1+x)$ around $x=0$ to approximate the regularizer in (13), which converges when the singular values of $J_g(h(x))$ are smaller than $\sqrt{\beta}$. Restricting the Taylor series to just first order term yields the simplified regularizer of $\frac{1}{2}\|J_g(h(x))\|_F^2$ (note that this approximation is crude: β cancels out and does not influence the decoder regularizer in any way). Similar approximations can be obtained for (12) which will yield the regularizer of $\|J_g(h(x))[-H_{p_x}(g(h(x)))]^{1/2}\|_F^2$. This simplified regularizer of $\frac{1}{2}\|J_g(h(x))\|_F^2$ weighted by a free hyperparameter has been used in a few earlier works with autoencoders, including recently in (Ghosh et al., 2019), where it was motivated in a rather heuristic manner for encouraging smoothness. On the other hand, we are specifically motivated by uncovering the regularization implicit in β -VAE and the regularizer in (13) emerges as part of this analysis.

6. Related Work

Our work resembles existing work on marginalizing out noise to obtain deterministic regularizers. Maaten et al. (2013) proposed deterministic regularizers obtained with marginalizing feature noise belonging to exponential family distributions. Chen et al. (2012) marginalize noise in denoising autoencoders to learn robust representations. Marginalization of dropout noise has also been explored in the context of linear models as well as deep neural networks (Srivastava, 2013; Wang & Manning, 2013; Srivastava et al., 2014; Poole et al., 2014). Recently, Ghosh et al. (2019) argued for replacing stochasticity in VAEs with deterministic regularizers resulting in deterministic regularized autoencoder objectives. However, the regularizers considered there were motivated from a heuristic perspective of encouraging smoothness in the decoding model. Another recent work (Kumar et al., 2019) uses injective probability flow to derive regularized autoencoding objectives with Jacobian based regularizers. On the other hand, our goal in Sec. 4 is to specifically uncover the regularizers implicit in β -VAE objective, and the regularizers in (4), (7), (12) and (13) are derived by explicitly marginalizing out noise coming from the posterior and then solving for the optimal posterior covariance.

Our work is also related to a recent work by Rolinek et al. (2019) that considered the case of VAEs with Gaussian prior, Gaussian posterior with diagonal covariance and Gaussian observations, and showed that diagonal posterior covariance encourages the decoder Jacobian to have orthogonal columns. However, we explicitly characterize the regularization effect of posterior covariance, obtaining insights into the effect of sparsity structure of the posterior precision matrix $\Sigma_{z|x}^{-1}$ on the decoder Jacobian (Eq. (11)). This leads us to obtain regularized autoencoder objectives with specific

regularizers (e.g., Eq. (12)). Our analysis also generalizes to observation models other than Gaussian. Stühmer et al. (2019) recently studied structured non-Gaussian priors for unsupervised disentanglement, motivated by rotational non-uniqueness issues associated with isotropic Gaussian prior.

7. Experiments

We conduct experiments on MNIST (Lecun et al., 1998) and CelebA (Liu et al., 2015) to empirically test the closeness of the proposed deterministic regularized objective to the original β -VAE objective and the relation between the posterior covariance and the Jacobian of the decoder. We use Gaussian distributions for the prior, variational posterior, and observation model in all our experiments for both β -VAE and the proposed deterministic objectives (which reduces to the GRAE objective of Eq. (13) for the Gaussian case). Note that for the Gaussian observation model, multiplication by β for the KL term in β -VAE is equivalent to assuming an isotropic decoding covariance of $\frac{1}{\beta}I$ in a VAE. We use 64×64 cropped images for CelebA faces as used in several earlier works. We use 5 layer CNN architecture for both encoder and decoder, with decoder layers consisting of transposed convolutions. We use the elu activations (Clevert et al., 2015) in all hidden layers of encoder and decoder. We use elu to test the approximation quality of GRAE objective when Eq. (6) is not exact. For piecewise-linear activations such as relu, Eq. (6) is exact and the approximation can only get better compared to elu. The same architecture is used for both β -VAE and GRAE, except we use an extra fully-connected (fc) output layer in the encoder for β -VAE to output the standard deviations of the mean field variational posteriors. For non-factorized Gaussian posteriors, we mainly work with block-diagonal covariance matrices, thus also restricting the posterior precision matrix to be block-diagonal. This is implemented by an additional fc layer in the encoder outputting the entries of the appropriate Cholesky factors $C_{z|x}$ such that $\Sigma_{z|x} = C_{z|x}C_{z|x}^T$ is block diagonal with desired block sizes. All MNIST and CelebA models are trained for 20k and 50k iterations respectively, using the Adam optimizer (Kingma & Ba, 2014).

Relation between posterior covariance and Jacobian structure. Based on the relation in Eq. (11), we expect to see similar block diagonal structures in $\Sigma_{z|x}^{-1}$ (or $\Sigma_{z|x}$) and $J_g(h(x))^T J_g(h(x))$. Figure 2 visualizes these two matrices for a few test points for different values of β , latent dimensionality d , and block size b . In many cases, these two matrices stay close to each other.

Comparing the β -VAE and GRAE objectives. We empirically compare the values of the β -VAE (minimization) objective (2), its Taylor approximation (7), and the GRAE objective (13) to test their closeness. We train the same encoder-decoder architecture as above, using Gaus-

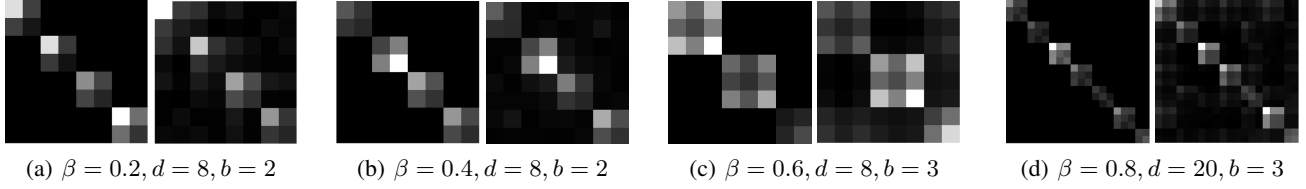


Figure 2. MNIST: Posterior precision matrices $\Sigma_{z|x}^{-1}$ (left) and the corresponding $J_g(h(x))^T J_g(h(x))$ (right), for different values of β and latent dimensionality d . Block size b for the posterior covariance was taken to be 2 or 3. More plots are shown in Appendix.

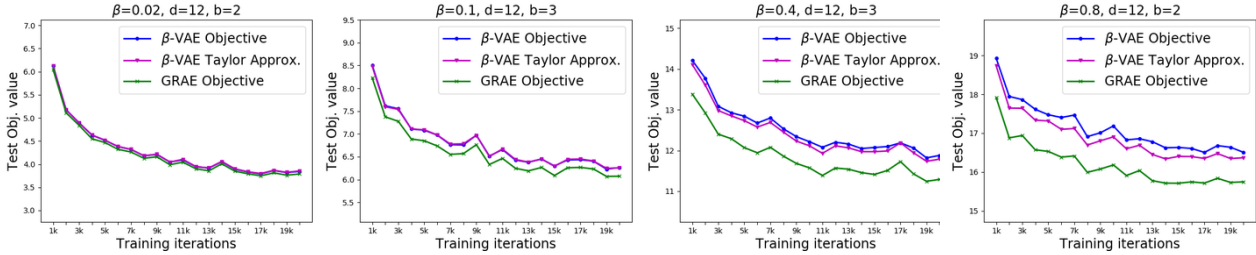


Figure 3. MNIST: Comparison of objective values of β -VAE, its Taylor approximation (Eq. (7)), and GRAE (Eq. (13)) for different values of β and block size b for posterior covariance matrix. Latent dimensionality d is fixed to 12. More plots can be viewed in the Appendix.

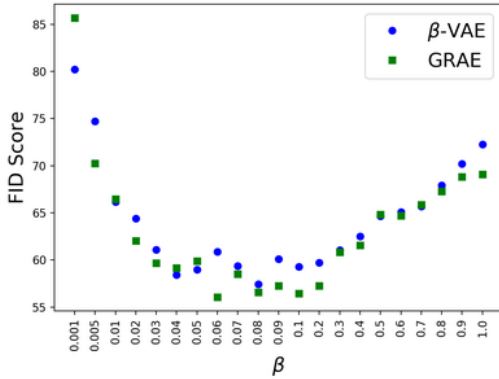


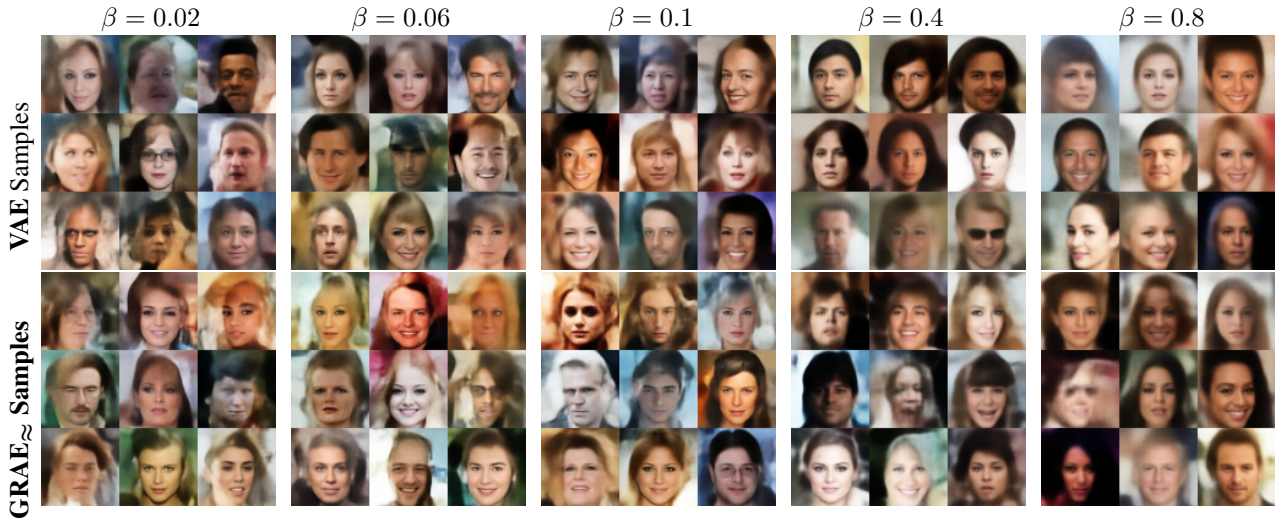
Figure 4. FID scores for CelebA generated samples using β -VAE and GRAE_{\approx} : averaged over 5 runs for each β . Samples from the two models stay close in terms of FID scores, further substantiating the validity of our derived deterministic approximation.

sian prior, Gaussian posterior and Gaussian observations, on the β -VAE objective while using a single sample approximation for the expectation term $\mathbb{E}_{q(z|x)} \log p(x|z)$. We evaluate all three objectives on a fixed held-out test set of 5000 examples as the training iterations proceed. Fig. 3 shows the comparison of the three objectives for MNIST. The objectives stay close to each other for a reasonably wide range of β values, with the gap between them decreasing for smaller β values. The gap between the β -VAE Taylor approximation and GRAE objectives increases more rapidly with β than the gap between β -VAE and its Taylor approximation. This gap is analyt-

ically given by $\frac{\beta}{2} [\text{tr}(I + \frac{1}{\beta} J_g(h(x))^T J_g(h(x)) \Sigma_{z|x}) - \log |(I + \frac{1}{\beta} J_g(h(x))^T J_g(h(x)) \Sigma_{z|x}) - d|]$, which vanishes when Eq. (11) holds exactly. Although these gaps increase with larger β , we observe that the trend of the three objectives is still strikingly similar. We provide more comparison plots in the Appendix.

Training models using the GRAE_{\approx} objective. Next, we test how the GRAE objective behaves when used for training. As discussed earlier, we use a stochastic approximation of Eq. (14) for the decoder regularizer to train the model (referred as GRAE_{\approx} objective). We work with CelebA 64×64 images and use standard Gaussian prior with latent dimensionality of 128, Gaussian observations, and factored Gaussian posterior. Table 1 shows the decoded samples from standard normal prior for both GRAE_{\approx} and β -VAE trained with different values of β . It can be noted that the generated samples follow similar trend qualitatively for both β -VAE and GRAE_{\approx} , with large β values resulting in more blurry samples. This provides an evidence for validity of GRAE_{\approx} as a training objective that behaves similar to β -VAE. As an attempt to quantify the similarity, we also compare the FID scores of the generated samples for both models as a function of β in Fig. 4. The FID scores stay close for both models, particularly for $\beta \geq 0.01$ where sample quality is better (*i.e.*, lower FID scores). This further empirically substantiates the faithfulness of our derived deterministic approximation. As future work, it will be interesting to explore other tractable approximations to the GRAE objective and different weights for the encoder regularizer and decoder regularizer (which are both currently

Table 1. CelebA samples using the standard normal prior for β -VAE and GRAE_{\approx} (Eq. (13) with the regularizer approximated by stochastic approximation of the upper bound of Eq. (14)) for different values of β . Samples from models trained using the GRAE_{\approx} objective have similar smoothness/blurriness as samples from β -VAE models for a wide range of β . More samples can be viewed in the Appendix.



fixed to $\beta/2$ in the GRAE objective).

8. Conclusion

We studied regularization effects in β -VAE from two perspectives: (i) analyzing the role that the choice of variational family can play in influencing the uniqueness properties of the solutions, and (ii) characterizing the regularization effect of the variational posterior on the decoding model by integrating out the posterior noise in an approximate objective. The second perspective leads to deterministic regularized autoencoding objectives for the case of location-scale posteriors and priors. Our analysis helps in connecting β -VAE and regularized autoencoders in a more principled manner, and we hope that this will help to motivate novel regularizers for autoencoding objectives.

Acknowledgements. We would like to thank Alex Alemi and Andrey Zhmoginov for providing helpful comments on the manuscript. We also thank Matt Hoffman and Kevin Murphy for insightful discussions.

References

- Adamčík, M. The information geometry of bregman divergences and some applications in multi-expert reasoning. *Entropy*, 16(12), 2014.
- Alemi, A. A., Poole, B., Fischer, I., Dillon, J. V., Saurous, R. A., and Murphy, K. Fixing a broken elbow. *arXiv preprint arXiv:1711.00464*, 2017.
- Arvanitidis, G., Hansen, L. K., and Hauberg, S. Latent space oddity: on the curvature of deep generative models. *arXiv preprint arXiv:1710.11379*, 2017.
- Bengio, Y., Courville, A., and Vincent, P. Representation learning: A review and new perspectives. *IEEE transactions on pattern analysis and machine intelligence*, 35(8): 1798–1828, 2013.
- Burgess, C. P., Higgins, I., Pal, A., Matthey, L., Watters, N., Desjardins, G., and Lerchner, A. Understanding disentangling in β -vae. *arXiv preprint arXiv:1804.03599*, 2018.
- Chen, M., Xu, Z., Weinberger, K., and Sha, F. Marginalized denoising autoencoders for domain adaptation. *arXiv preprint arXiv:1206.4683*, 2012.
- Chen, N., Klushyn, A., Kurle, R., Jiang, X., Bayer, J., and van der Smagt, P. Metrics for deep generative models. *arXiv preprint arXiv:1711.01204*, 2017.
- Chen, T. Q., Li, X., Grosse, R. B., and Duvenaud, D. K. Isolating sources of disentanglement in variational autoencoders. In *Advances in Neural Information Processing Systems*, pp. 2610–2620, 2018.
- Clevert, D.-A., Unterthiner, T., and Hochreiter, S. Fast and accurate deep network learning by exponential linear units (elus). *arXiv preprint arXiv:1511.07289*, 2015.
- Darmois, G. Analyse des liaisons de probabilité. In *Proc. Int. Stat. Conferences 1947*, pp. 231, 1951.
- Darmois, G. Analyse générale des liaisons stochastiques: étude particulière de l’analyse factorielle linéaire. *Revue de l’Institut international de statistique*, pp. 2–8, 1953.

- Ghosh, P., Sajjadi, M. S. M., Vergari, A., Black, M., and Schölkopf, B. From variational to deterministic autoencoders, 2019.
- Gilpin, L. H., Bau, D., Yuan, B. Z., Bajwa, A., Specter, M., and Kagal, L. Explaining explanations: An overview of interpretability of machine learning. In *2018 IEEE 5th International Conference on data science and advanced analytics (DSAA)*, pp. 80–89. IEEE, 2018.
- Higgins, I., Matthey, L., Pal, A., Burgess, C., Glorot, X., Botvinick, M., Mohamed, S., and Lerchner, A. beta-vaes: Learning basic visual concepts with a constrained variational framework. In *International Conference on Learning Representations*, 2017.
- Hyvärinen, A. and Pajunen, P. Nonlinear independent component analysis: Existence and uniqueness results. *Neural Networks*, 12(3):429–439, 1999.
- Kim, H. and Mnih, A. Disentangling by factorising. *arXiv preprint arXiv:1802.05983*, 2018.
- Kingma, D. and Ba, J. Adam: A method for stochastic optimization. *arXiv preprint arXiv:1412.6980*, 2014.
- Kingma, D. P. and Welling, M. Auto-encoding variational bayes. *arXiv preprint arXiv:1312.6114*, 2013.
- Kuhnel, L., Fletcher, T., Joshi, S., and Sommer, S. Latent space non-linear statistics. *arXiv preprint arXiv:1805.07632*, 2018.
- Kumar, A., Sattigeri, P., and Balakrishnan, A. Variational inference of disentangled latent concepts from unlabeled observations. In *ICLR*, 2018.
- Kumar, A., Poole, B., and Murphy, K. Learning generative samplers using relaxed injective flow. In *ICML Workshop on Invertible Neural Nets and Normalizing Flows*, 2019.
- Lecun, Y., Bottou, L., Bengio, Y., and Haffner, P. Gradient-based learning applied to document recognition. In *Proceedings of the IEEE*, pp. 2278–2324, 1998.
- Liu, Z., Luo, P., Wang, X., and Tang, X. Deep learning face attributes in the wild. In *Proceedings of the IEEE International Conference on Computer Vision*, pp. 3730–3738, 2015.
- Locatello, F., Bauer, S., Lucic, M., Gelly, S., Schölkopf, B., and Bachem, O. Challenging common assumptions in the unsupervised learning of disentangled representations. In *ICML*, 2019.
- Lukacs, E., King, E. P., et al. A property of the normal distribution. *The Annals of Mathematical Statistics*, 25(2):389–394, 1954.
- Maaten, L., Chen, M., Tyree, S., and Weinberger, K. Learning with marginalized corrupted features. In *International Conference on Machine Learning*, pp. 410–418, 2013.
- Mathieu, E., Rainforth, T., Siddharth, N., and Teh, Y. W. Disentangling disentanglement in variational autoencoders. In *International Conference on Machine Learning*, pp. 4402–4412, 2019.
- Peters, J., Janzing, D., and Schölkopf, B. *Elements of causal inference: foundations and learning algorithms*. MIT press, 2017.
- Poole, B., Sohl-Dickstein, J., and Ganguli, S. Analyzing noise in autoencoders and deep networks, 2014.
- Rezende, D. J., Mohamed, S., and Wierstra, D. Stochastic backpropagation and approximate inference in deep generative models. *arXiv preprint arXiv:1401.4082*, 2014.
- Rolinek, M., Zietlow, D., and Martius, G. Variational autoencoders pursue pca directions (by accident). In *Proceedings of the IEEE Conference on Computer Vision and Pattern Recognition*, pp. 12406–12415, 2019.
- Sason, I. and Verdú, S. f -divergence inequalities. *IEEE Transactions on Information Theory*, 62(11):5973–6006, 2016.
- Shao, H., Kumar, A., and Thomas Fletcher, P. The riemannian geometry of deep generative models. In *Proceedings of the IEEE Conference on Computer Vision and Pattern Recognition Workshops*, pp. 315–323, 2018.
- Shu, R., Bui, H. H., Zhao, S., Kochenderfer, M. J., and Ermon, S. Amortized inference regularization. In *Advances in Neural Information Processing Systems*, pp. 4393–4402, 2018.
- Skitovitch, V. On a property of the normal distribution. *DAN SSSR*, 89:217–219, 1953.
- Srivastava, N. Improving neural networks with dropout. *University of Toronto*, 182:566, 2013.
- Srivastava, N., Hinton, G., Krizhevsky, A., Sutskever, I., and Salakhutdinov, R. Dropout: a simple way to prevent neural networks from overfitting. *The journal of machine learning research*, 15(1):1929–1958, 2014.
- Stühmer, J., Turner, R. E., and Nowozin, S. Independent subspace analysis for unsupervised learning of disentangled representations. *arXiv preprint arXiv:1909.05063*, 2019.
- Tipping, M. E. and Bishop, C. M. Probabilistic principal component analysis. *Journal of the Royal Statistical Society: Series B (Statistical Methodology)*, 61(3):611–622, 1999.

van Steenkiste, S., Locatello, F., Schmidhuber, J., and Bachem, O. Are disentangled representations helpful for abstract visual reasoning?, 2019.

Wang, S. and Manning, C. Fast dropout training. In *international conference on machine learning*, pp. 118–126, 2013.

Zhu, J., Chen, N., and Xing, E. P. Bayesian inference with posterior regularization and applications to infinite latent svms, 2012.

Appendix.

Here we provide more details, in particular:

Appendix A: proof of Theorem 1

Appendix B: experiments to empirically verify the uniqueness results

Appendix C: architecture details for encoder and decoder

Appendix D: plots visualizing the approximate posterior precision matrix $\Sigma_{z|x}^{-1}$ and $J_g(h(x))^\top J_g(h(x))$ to verify the relation in Eq. (11)

Appendix E: plots comparing objective values of β -VAE and GRAE

Appendix F: comparison of samples from β -VAE and GRAE $_{\approx}$

A. Uniqueness in β -VAE

We provide the proof of Theorem 1 which states that any β -VAE solution obtained by transforming the generative model of the optimal solution while keeping the prior and the marginal log-likelihood same, will result in decreasing the objective value.

Theorem 1. *Let R be the class of mixing transforms that leave the prior invariant, and p_r be the generative model obtained by transforming the latents of the model p by $r \in R$. Let $L(q^*, p^*) = \max_{q \in \mathcal{Q}, p \in \mathcal{P}} L(q, p)$. Let $\tilde{\mathcal{Q}}$ be the completion of \mathcal{Q} by R , i.e., $\tilde{\mathcal{Q}} = \{r\#q : q \in \mathcal{Q}, r \in R\} \cup \mathcal{Q}$. If \mathcal{Q} is s.t. $q \in \mathcal{Q} \Rightarrow r\#q \notin \mathcal{Q}$ for all $r \in R$, and $\arg \max_{q \in \tilde{\mathcal{Q}}} L(q, p^*)$ is unique, then $\max_{q \in \mathcal{Q}} L(q, p_r^*) < L(q^*, p^*)$.*

Proof. The objective after transforming a model p with $r \in R$ yields:

$$\begin{aligned}
L(q, p_r) &:= \mathbb{E}_{q(z|x)} \log p_{x|z}(x|r(z)) - \beta \text{KL}(q(z|x) \| p_z(z)) \\
&= \int \log \left(p_{x|z}(x|r(z)) \left(\frac{p_z(z)}{q(z|x)} \right)^\beta \right) q(z|x) dz \\
&= \int \log \left(p_{x|z}(x|z') \left(\frac{p_z(r^{-1}(z'))}{q(r^{-1}(z')|x)} \right)^\beta \right) q(r^{-1}(z')|x) dz' \\
&= \int \log \left(p_{x|z}(x|z) \left(\frac{p_z(z)}{q(r^{-1}(z)|x)} \right)^\beta \right) q(r^{-1}(z)|x) dz \\
&= \mathbb{E}_{q_r} \log p_{x|z}(x|z) - \beta \text{KL}(q_r \| p_z) = L(q_r, p).
\end{aligned} \tag{15}$$

where we used the shorthand q_r to denote the transformed variational density $r\#q_{z|x}$. This also implies that $L(q, p) = L(q_{r^{-1}}, p_r)$. Hence, the optimum value of the β -VAE objective $L(q^*, p^*) = L(q_{r^{-1}}^*, p_r^*) \forall r \in R$. Choosing \mathcal{Q} such that $q \in \mathcal{Q} \Rightarrow r\#q \notin \mathcal{Q} \forall r \in R$ will ensure that $q_{r^{-1}}^* \notin \mathcal{Q}$. Note that optimizing the β -VAE objective over $\tilde{\mathcal{Q}} = \{r\#q :$

$q \in \mathcal{Q}, r \in R\}$ does not change the optimal value, i.e., $L(q^*, p^*) = \max_{q \in \mathcal{Q}, p \in \mathcal{P}} L(q, p) = \max_{q \in \tilde{\mathcal{Q}}, p \in \mathcal{P}} L(q, p)$. The statement of the theorem can now be proven by contradiction. Suppose $\exists q' \in \mathcal{Q}$ s.t. $L(q', p_r^*) = L(q_r^*, p^*) \geq L(q^*, p^*)$. However, this will contradict the assumption that $q^* = \arg \max_{q \in \tilde{\mathcal{Q}}} L(q, p^*)$ and that it is unique. Hence $\forall q' \in \mathcal{Q}, L(q', p_r^*) < L(q^*, p^*)$. \square

Corollary 2. *If the set $\tilde{\mathcal{Q}}$ defined in Theorem 1 is convex, then $\arg \max_{q \in \tilde{\mathcal{Q}}} L(q, p^*)$ is unique. When all other assumptions of Theorem 1 are met, we have $\max_{q \in \mathcal{Q}} L(q, p_r^*) < L(q^*, p^*)$.*

Proof. As the β -VAE objective is strongly concave in q (first term is linear in q and the KL-divergence term is strongly convex in q (Adamčík, 2014; Sason & Verdu, 2016)), optimizing it over a convex set $\tilde{\mathcal{Q}}$ for a fixed p will have a unique maximizer. Hence, the result of Theorem 1 holds when all other assumptions are met. \square

B. Uniqueness in β -VAE: empirical results

Here we provide more details on simulations we perform to verify that appropriately choosing the variational family \mathcal{Q} imparts uniqueness to the β -VAE (or plain VI) solution with respect to the corresponding class of transformations R . We consider the case of \mathcal{Q} being mean-field distributions and R being rotations. We work with two dimensional data so that rotations can be represented by a scalar (angle of planar rotation) which can be plotted conveniently.

We generate 4k samples in two dimensions by the generative model $x = \nu(Wz) + \epsilon$, with $z \sim \mathcal{N}(0, I_{2 \times 2})$, $\epsilon \sim \mathcal{N}(0, .05^2 I_{2 \times 2})$. Entries of $W \in \mathbb{R}^{2 \times 2}$ are sampled from $\mathcal{N}(0, I_{2 \times 2})$ and normalized such that columns have different ℓ_2 norms (2 and 1, respectively). The function ν acts elementwise on the vector and is taken to be either Identity (reducing it to Probabilistic PCA) or a nonlinearity (tanh, sigmoid, elu). A VAE is learned on this data, with the decoder of the same form as the generative model, i.e., $x = \nu(Az) + b$, and variational posterior of the form $q(z|x) = \mathcal{N}(Cx + d, \Sigma)$ with A, b, C, d and Σ learned. We also do unamortized variational inference with the variational distribution $q_i(z) = \mathcal{N}(\mu_i, \Sigma_i)$ for the i 'th data point ($\mu_i \in \mathbb{R}^2, \Sigma_i \in S_+^2$). For the case of mean-field variational inference, we learn only diagonal elements of Σ or Σ_i that appear in the objective (ELBO), leaving the off-diagonal elements free. We do multiple runs of this experiment by randomizing over W, ϵ, z for the true generative model of data and randomizing over the initializations of the VAE parameters. For each run, we measure the rotation angle between the true latents and the inferred posterior means. Rotation angle is computed after ignoring permutation and reflection of axes so the angle ranges in $(-45, 45]$ degrees with -45 degree rotation being same as 45 degree rotation.

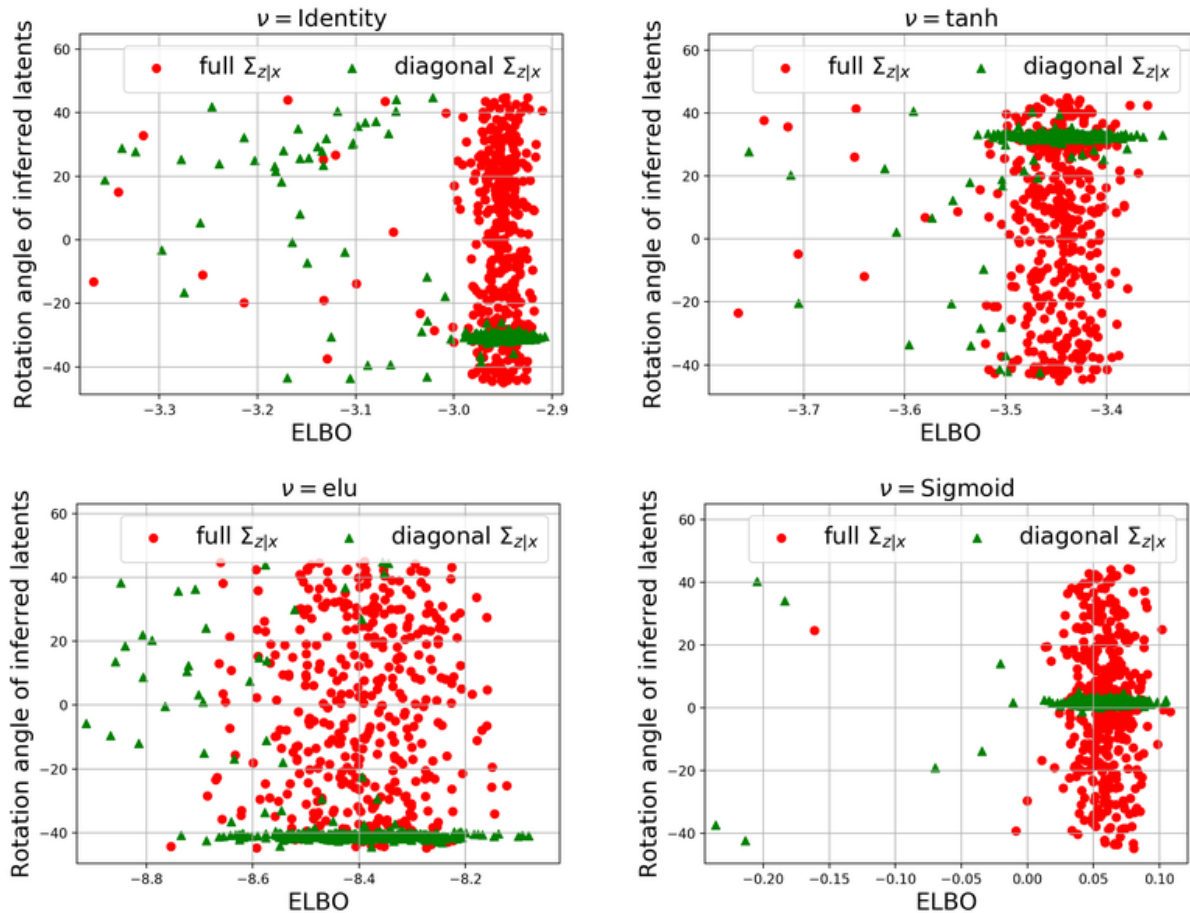


Figure 5. Rotation angle between true latents and inferred latents with VAEs (multiple runs): The true generative model for the data is $x = \nu(Wz) + \epsilon$, with $z \sim \mathcal{N}(0, I_{2 \times 2})$, $\epsilon \sim \mathcal{N}(0, .05^2 I_{2 \times 2})$. Diagonal Σ encourages unique solution in terms of inferred latents as the ELBO increases. Please refer to the text for more details.

We train the model parameters by gradient descent (use all data samples for a gradient update). The learning rate is set to 0.1 in the beginning and is reduced in a stepwise manner after every n iterations by a factor of 10, till the learning rate reaches 10^{-5} (*i.e.*, each model is trained for $5n$ iterations). To train models up to varying degree of optimality, we take n to be $\{100, 500, 1k, 2k, 3k, 4k, 5k, 6k, 7k, 8k, 9k, 10k, 20k\}$. We do 20 random trials for each value of n from 100 to 9k, and 100 random trials for $n = 10k$ and $n = 20k$ (total 420 random trials per experiment).

We also take special care in how we parameterize the models so that the implicit bias of gradient descent does not affect the solution in any particular way. For amortized inference with VAE, we parameterize encoder parameters as $C = O_1 C'$ and $\Sigma = O_2 D' D'^T O_2^T$, where O_1, O_2 are random 2×2 rotation matrices that are fixed at the beginning of training (different for each random trial), and C' and D' are the parameters learned by gradient descent. For unamortized variational inference, we again parameterize

$\Sigma_i = O D'_i D_i'^T O^T$ with O being a random 2×2 rotation matrix and D'_i being the trainable parameters. We notice that without these reparameterizations, implicit bias of gradient descent can impart some degree of uniqueness to the model, which we particularly noticed in the case of unamortized inference.

Fig. 5 shows the scatter plots of rotation angle vs ELBO for the amortized case (VAE) with $\nu = \text{identity, tanh, elu, sigmoid}$. Having diagonal Σ (mean-field $q(z|x)$) encourages unique solution in terms of inferred latents as the ELBO increases (ignoring the permutations and reflections of latent axes).

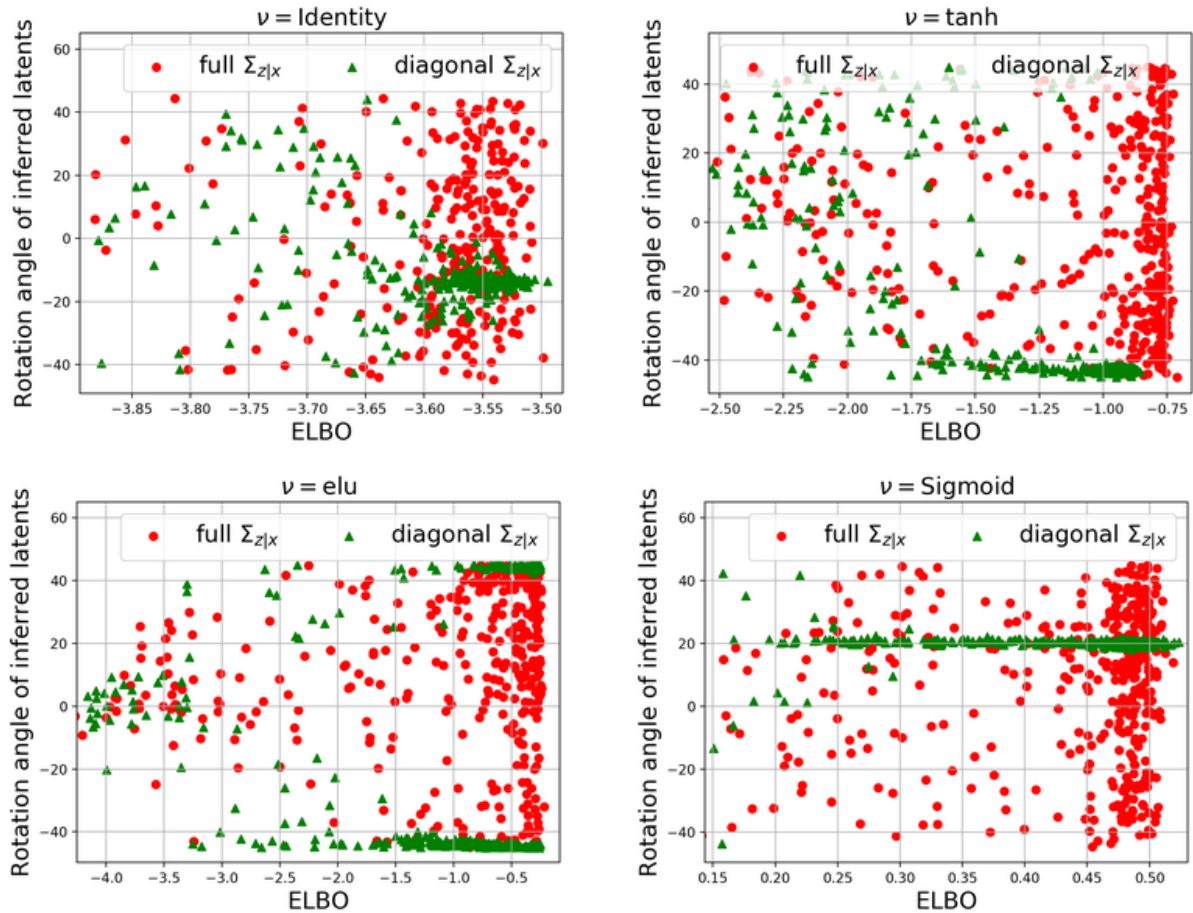


Figure 6. Rotation angle between true latents and inferred latents with unamortized variational inference (multiple runs): The true generative model for the data is $x = \nu(Wz) + \epsilon$, with $z \sim \mathcal{N}(0, I_{2 \times 2})$, $\epsilon \sim \mathcal{N}(0, .05^2 I_{2 \times 2})$. Diagonal Σ encourages unique solution in terms of inferred latents as the ELBO increases. Please refer to the text for more details.

C. Architectures

Here we describe the architecture for our MNIST and CelebA models. We list Conv (convolutional) and ConvT (transposed convolution) layers with their number of filters, kernel size, and stride. Latent dimension for CelebA is fixed to be 128 in all experiments, and the dimension for MNIST experiments is varied in the set $\{8, 12, 16, 20\}$. The architecture is shown for the GRAE model. For β -VAE, the encoder has an extra output through an fully-connected layer for standard deviations of the posterior factors in the case of mean-field posterior, or for the elements of the Cholesky factor in the case of block-diagonal posterior covariance matrices.

| MNIST | CelebA |
|---|---|
| Encoder | |
| $x \in \mathcal{R}^{28 \times 28}$ | $x \in \mathcal{R}^{64 \times 64 \times 3}$ |
| \rightarrow Conv _{64,4,1} \rightarrow BN \rightarrow ELU | \rightarrow Conv _{128,5,1} \rightarrow BN \rightarrow ELU |
| \rightarrow Conv _{128,4,2} \rightarrow BN \rightarrow ELU | \rightarrow Conv _{256,5,2} \rightarrow BN \rightarrow ELU |
| \rightarrow Conv _{256,4,2} \rightarrow BN \rightarrow ELU | \rightarrow Conv _{512,5,2} \rightarrow BN \rightarrow ELU |
| \rightarrow Conv _{512,4,2} \rightarrow BN \rightarrow ELU | \rightarrow Conv _{1024,5,2} \rightarrow BN \rightarrow ELU |
| \rightarrow Conv _{512,4,1} \rightarrow BN \rightarrow ELU | \rightarrow Conv _{1024,5,2} \rightarrow BN \rightarrow ELU |
| \rightarrow Flatten \rightarrow FC _{d} | \rightarrow Flatten \rightarrow FC ₁₂₈ |
| Decoder | |
| $z \in \mathcal{R}^d \rightarrow$ FC _{7\times7\times256} | $z \in \mathcal{R}^{128} \rightarrow$ FC _{16\times16\times512} |
| \rightarrow BN \rightarrow ELU | \rightarrow BN \rightarrow ELU |
| \rightarrow ConvT _{512,4,1} \rightarrow BN \rightarrow ELU | \rightarrow ConvT _{1024,5,1} \rightarrow BN \rightarrow ELU |
| \rightarrow ConvT _{256,4,1} \rightarrow BN \rightarrow ELU | \rightarrow ConvT _{512,5,2} \rightarrow BN \rightarrow ELU |
| \rightarrow ConvT _{128,4,2} \rightarrow BN \rightarrow ELU | \rightarrow ConvT _{256,5,2} \rightarrow BN \rightarrow ELU |
| \rightarrow ConvT _{64,4,2} \rightarrow ELU | \rightarrow ConvT _{128,5,2} \rightarrow ELU |
| \rightarrow Conv _{1,4,1} \rightarrow Sigmoid | \rightarrow Conv _{3,5,1} \rightarrow Sigmoid |

D. Relation between posterior covariance and Jacobian structure

We provide more plots visualizing the approximate posterior precision matrix $\Sigma_{z|x}^{-1}$ and $J_g(h(x))^\top J_g(h(x))$ in Figure 7. Based on the relation in Eq. (11), we expect to see similar block diagonal structures in $\Sigma_{z|x}^{-1}$ (or $\Sigma_{z|x}$) and $J_g(h(x))^\top J_g(h(x))$.

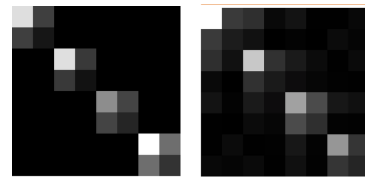
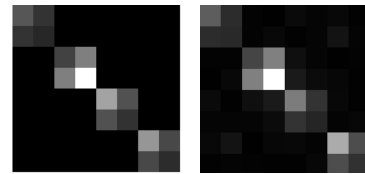
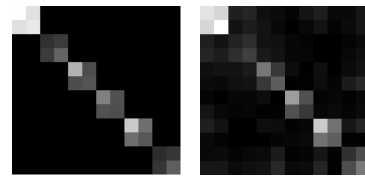
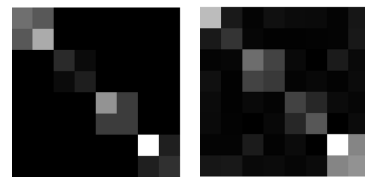
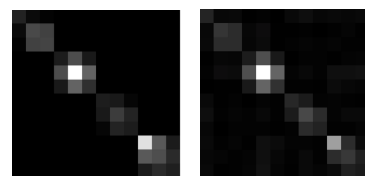
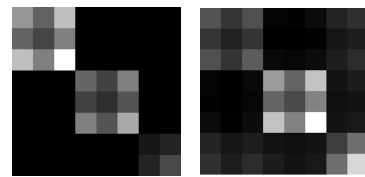
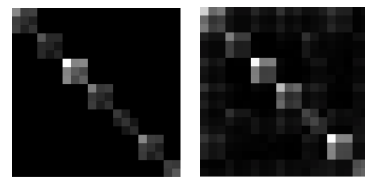
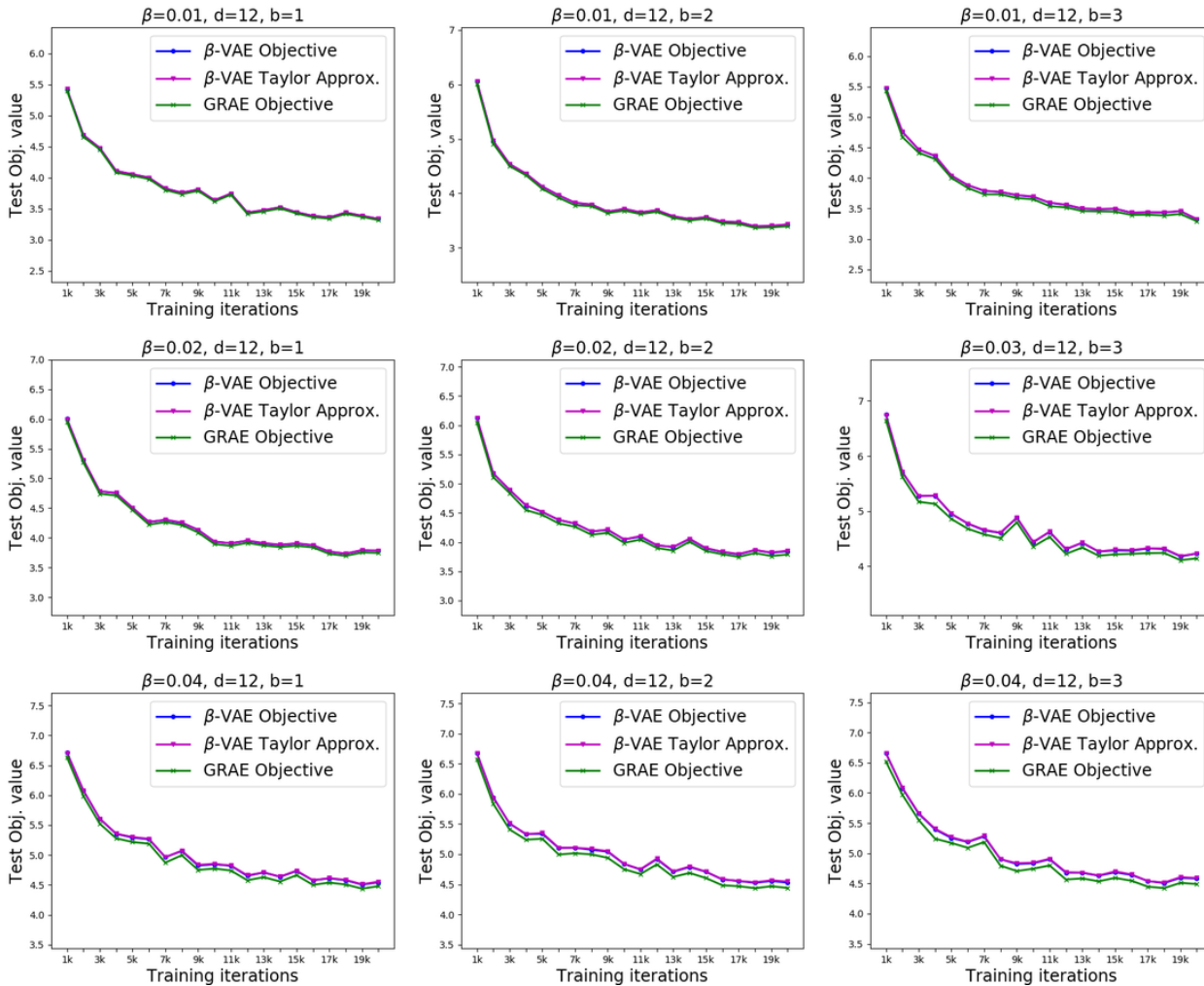
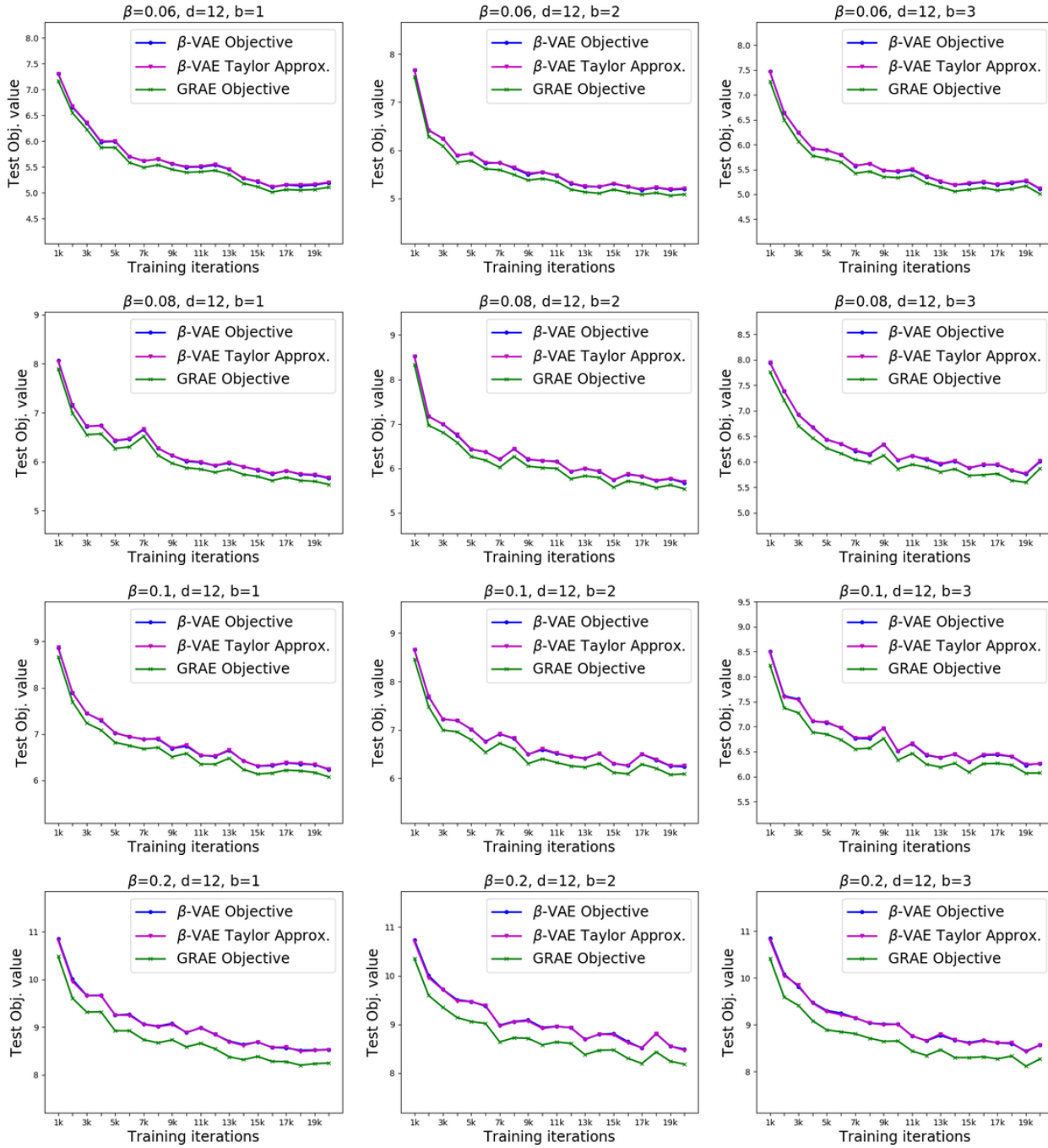
(a) $\beta = 0.2, d = 8, b = 2$ (b) $\beta = 0.4, d = 8, b = 2$ (c) $\beta = 0.6, d = 12, b = 2$ (d) $\beta = 1, d = 8, b = 2$ (e) $\beta = 0.4, d = 12, b = 3$ (f) $\beta = 0.6, d = 8, b = 3$ (g) $\beta = 0.8, d = 20, b = 3$

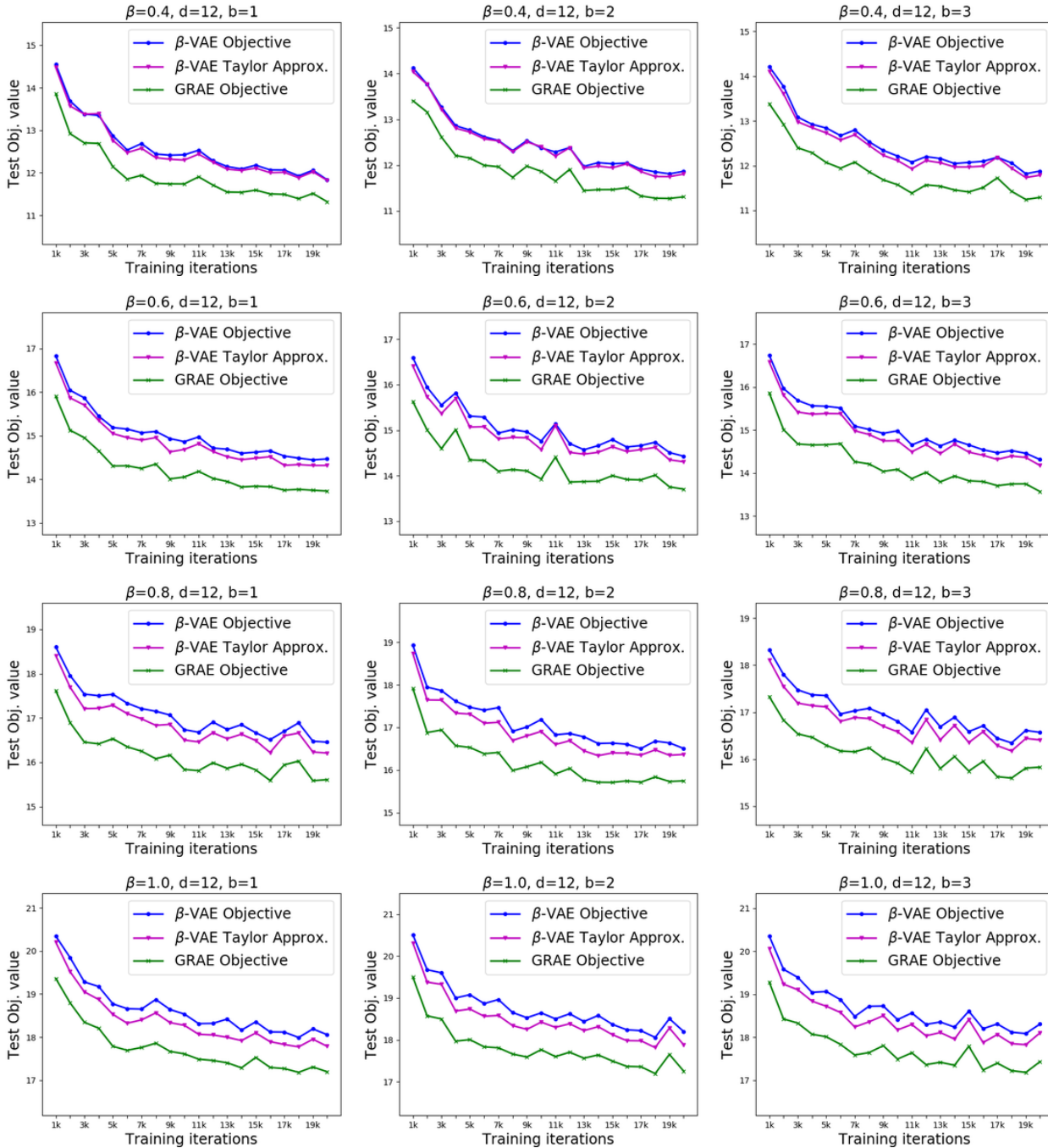
Figure 7. MNIST: Posterior precision matrices $\Sigma_{z|x}^{-1}$ (left) and the corresponding $J_g(h(x))^\top J_g(h(x))$ (right), for different values of β and latent dimensionality d . Block size b for the posterior covariance was taken to be 2 (top row) or 3 (bottom row).

E. Comparison of objective values

We show more plots comparing objective values of β -VAE, its Taylor series approximation, and the GRAE objective for various values of β on MNIST. The latent dimension d is fixed to 12, and the block-size b (for block-diagonal posterior covariance) is varied over $\{1, 2, 3\}$. The model is trained using the β -VAE objective and is evaluated on all objectives using a held-out test set of 5000 examples. As β increases, the gap between the β -VAE objective and its Taylor approximation increases. The gap between the Taylor approximation and the GRAE objective also increases with β . This gap is analytically given by $\frac{\beta}{2}[\text{tr}(I + \frac{1}{\beta} J_g(h(x))^\top J_g(h(x)) \Sigma_{z|x}) - \log |(I + \frac{1}{\beta} J_g(h(x))^\top J_g(h(x)) \Sigma_{z|x}) - d|]$.







F. Samples from VAE and GRAE

We visualize random CelebA samples using the standard normal prior for β -VAE and Gaussian-RAE for different values of β below. Note that for training the GRAE model, we actually minimize the stochastic approximation of the upper bound of Eq. (17) for the decoder regularizer. Hence we will refer to it as \approx GRAE. Samples from models trained using the GRAE objective have similar smoothness/blurriness as samples from β -VAE models, particularly for small β values.









